International Journal of Modern Manufacturing Technologies
ISSN 2067–3604, Vol. XVI, No. 3 / 2024
https://doi.org/ 10.54684/ijmmt.2024.16.3.136

DESIGN FOR ADDITIVE MANUFACTURING OF TOPOLOGICALLY OPTIMIZED AIR MANIFOLD

Nikolaos Kladovasilakis[1,2]

[1]Centre for Research and Technology Hellas – Information Technologies Institute (CERTH/ITI), Thessaloniki, 57001, Greece
[2]Digital Manufacturing and Materials Characterization Laboratory, School of Science and Technology, International Hellenic University, Thessaloniki, 57001, Greece

Corresponding author: Nikolaos Kladovasilakis, n.kladovasilakis@ihu.edu.gr

Abstract: Topology optimization is increasingly utilized in mechanical component design to achieve lightweight, cost-effective, and functional designs, facilitated by advanced design software and additive manufacturing technologies. This study presents a workflow for redesigning a low-pressure air manifold using cutting-edge design processes and Selective Laser Sintering (SLS) 3D printing with polyamide 12 (PA12). Through iterative finite element analyses (FEA), unnecessary material regions were removed and novel surface-architected materials were applied to critical areas to enhance its structural integrity. The final design, evaluated computationally under realistic conditions, demonstrated a weight reduction of up to 76% compared to the initial design, with production costs below €5 per item. The presented workflow provides a generic pipeline for the redesign and topology optimization processes of a manifold, which can be applicable to other similar 3D-printed mechanical parts derived from industries constructed either from metal or from polymer, such as hydraulic manifolds, nozzles, connectors, etc.
Key words: Design for Additive Manufacturing, Topology Optimization, Selective Laser Sintering, Air Manifold, Finite Element Analysis.

1. INTRODUCTION

Nowadays, several industries are exploring the integration of additive manufacturing (AM) processes into their production systems, either as replacements for conventional manufacturing equipment or in combination with them to enhance their manufacturability [1]. However, this approach often overlooks the unique opportunities presented by AM processes, primarily due to high-cost considerations and limitations in mass production. These challenges are prevalent across various advanced AM technologies, particularly in the Powder Bed Fusion (PBF) method [2].
The PBF method entails the use of fine plastic or metal powders with particle sizes smaller than 100μm, as feedstock material. The powder is spread on the building platform, and with the assistance of a laser or electron beam, it is sintered or melted according to the corresponding cross-section of the 3D print. Subsequently, the building platform descends, and the process is reiterated until the entire part is fabricated. The PBF method is capable of fabricating plastic and metal parts with high dimensional accuracy, reduced anisotropy, and improved mechanical properties comparable to those manufactured using conventional techniques, such as casting and machining [3]. Within the PBF method, various AM techniques are classified based on differences in feedstock material (plastic or metal) and power source (laser, electron beam, etc.). Table 1 provides an overview of these PBF techniques coupled with their corresponding feedstock materials.

Table 1. Existing PBF techniques along with their feedstock materials [3]

PBF technique	Feedstock material
Selective Laser Sintering (SLS)	Plastic (ABS, TPE, PA, TPU, etc.)
Selective Heat Sintering (SHS)	
Direct metal laser sintering (DMLS)	Metals and alloys (Titanium, Steel, Aluminium, etc.)
Selective Laser Melting (SLM)	
Electron Beam Melting (EBM)	

Despite the competitive advantages offered by the PBF method, two significant challenges must be addressed for its further adoption in industries [4,5]. The first challenge pertains to the mass production of 3D printed parts.

This obstacle is currently being addressed by manufacturers of 3D printers, who are developing equipment with larger build volumes and faster printing speeds. By leveraging these advancements, the productivity of 3D printers, particularly PBF ones capable of nesting and stacking 3D prints within their entire build volume, increases exponentially, enabling industries to establish clusters of 3D printers and achieve a production capacity of several hundred parts per day. The second obstacle is more complex and revolves around the overall cost of PBF processes. Apart from other process-related expenses such as power, maintenance, and material costs, PBF processes also necessitate pre-processing and post-processing labor for powder management, significantly increasing the overall process cost [6]. To mitigate this issue, the principle of design for additive manufacturing (DfAM) has been developed. DfAM, a subset of the broader design for manufacturing (DfM) concept, aims to extract product designs that are easily fabricable using AM technologies [7]. Over the past decade, numerous studies have investigated DfAM principles [8,9,10]. The consensus from these studies is that designs should undergo advanced topology optimization processes to reduce their mass/volume without compromising their structural integrity. In addition, the necessity for support geometry should be minimized by utilizing proper design tools such as chamfer, fillets, etc. Through DfAM, the geometry of 3D printed parts is optimized, reducing the required feedstock material and increasing productivity. Furthermore, DfAM ensures optimal part placement within the build volume, optimizing the total number of parts per print [11,12].

In this context, the present study aims to present an innovative framework for optimizing the design of part by combining DfAM and advanced topology optimization techniques. The aforementioned framework is presented through a practical case study of a low-pressure air manifold. More specifically, a commercial low-pressure air manifold was redesigned and topologically optimized to minimize its mass/volume withstanding the realistic operation conditions. Furthermore, surface-architected materials were employed on the outer surface of the manifold in order to enhance its mechanical response without significantly affecting the part's mass. All designed versions of the manifold were numerically evaluated under realistic conditions through Finite Element Analyses (FEA). Finally, each design was fabricated utilizing the PBF AM method, and more specifically SLS, to provide physical evidence of the feasibility and manufacturability of the produced designs. Figure 1 illustrates the flowchart of the current study.

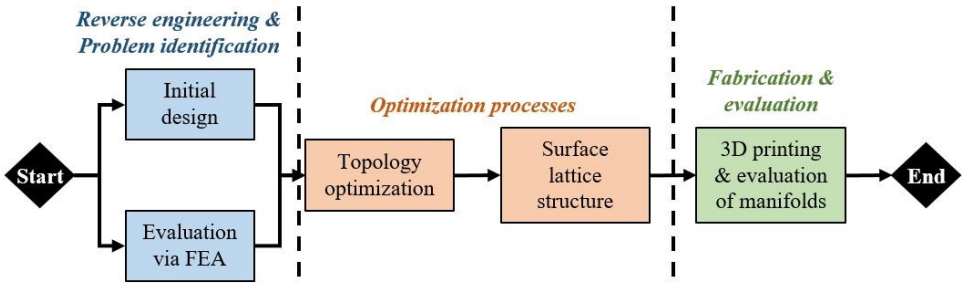

Fig. 1. Flowchart of the current study

2. MATERIALS AND METHODS

2.1. Case study identification

In the current study, the entire framework of DfAM was set on a case study of a commercial low-pressure air manifold. In detail, the aluminum block (part No. 90120) of the pneumatic RapidAir M3800 Maxline system was utilized. The retail price of this part is currently around 15-17 € [13]. This air manifold was designed to have four ports with three 3/8 and one 1/4 American National pipe tapered thread (NPT) and four mounting holes. It has a mass of 210.83 gr and is capable to withstand maximum air pressure of 13 bars. Figure 2 shows indicative images of the manifold along with its most crucial dimensions.

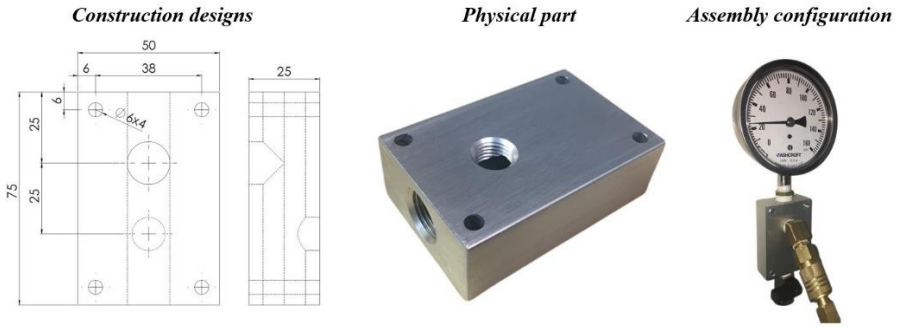

Fig. 2. Indicative images of manifold: construction designs, the physical part and assembly configuration

2.2. Design for additive manufacturing

Firstly, the idea was the replace construction material, i.e. the costly aluminum with industrial polyamide, such as PA12. PA12 is a thermoplastic polymer that exhibits excellent mechanical properties, including high tensile strength, impact resistance, toughness, and durability. The next step of DfAM was the identification of the employed AM technique. In the context of this paper, the SLS AM technique was utilized which is capable of producing complex geometry without the need of support. Therefore, topology optimization through a density-based approach was applicable. The density-based approach discretizes the part into a grid of elements, and the material density within each element is represented by a variable. The optimization process then iteratively adjusts these density variables via FEA iterations to redistribute material throughout the domain, typically guided by predefined design objectives and constraints [14,15]. The primary objective of this approach is to maximize the stiffness-to-weight ratio of the part. After the topology optimization process, the design was integrated with proper fillets to address undesired deformations due to the occurred thermal stresses. Finally, the present study applied one more novel step in the design process to enhance the part's mechanical response without significantly affecting the part's volume/mass. This step involved the employment of a surface lattice structure on the outer surface of the manifold, which concentrates the high stresses [16,17]. In detail, a conformable triangular honeycomb architected material with unit cell configuration of 7mm x 7mm x 2mm and strut thickness of 1mm was used. The dimensions of the employed architected material were selected in order to cover sufficiently the desired surface and ensure printability, i.e. without creating small cavities that will entrap un-sintered powder particles. It is worth mentioning that for the design process of the initial manifold the SolidWorks design platform was used. Moreover, for the topology optimization process, architected material integration and the smoothing processes the nTopology software was employed. Figure 3 portrays indicative images of a triangular honeycomb unit cell and a conformable configuration of the applied surface architected material.

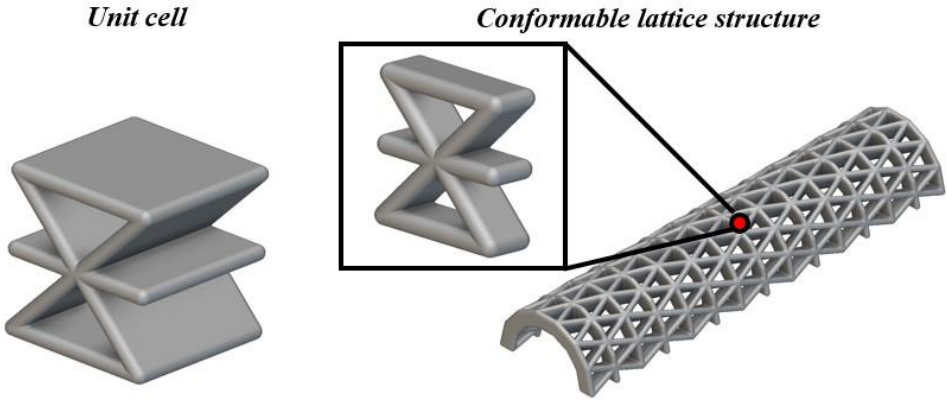

Fig. 3. Indicative images of a unit cell and employed conformable configuration for triangular honeycomb architected material

2.3. Additive manufacturing methodology

As it was aforementioned, the SLS technique of the PBF category was selected as employed additive manufacturing technology. In detail, the Lisa Sinterit SLS 3D printer (Sinterit™, Poland) was utilized for the fabrication of the optimized manifold. All 3D prints were manufactured with fine PA12 Sinterit powder which has a particle size distribution of D10 < 25.5 μm, D50 < 33μm and D90 < 42.5μm. It is worth noting that the employed powder was used for the first time and was labeled from the manufacturer as ready-to-print powder. For the process-related parameters, the indicative material profile of the manufacturer was followed adjusting the layer height at 0.075mm in order to achieve the optimum quality. Finally, according to the results of a previous study [18], this material profile extracts the properties, that are listed in Table 2, for the as-built 3D prints.

Table 2. Basic properties of as-built PA12 3D prints [18]

Properties	**Values**
Density	0.95 g/cm^3
Poisson ratio	0.37
Elastic modulus	938 ± 30 MPa
Yield strength	22.7 ± 0.5 MPa
Ultimate tensile strength (UTS)	31.8 ± 0.5 MPa
Elongation at break	13 ± 1 %

2.4. Finite Element Model (FEM)

For the evaluation of the commercial and the developed manifold's design, the proper Finite Element Model (FEMs) was developed. More specifically, the ANSYS™ software (ANSYS, Inc., Canonsburg, Pennsylvania, U.S.) via the static module, was used in order to simulate the operation of the air manifold under steady conditions [19]. Regarding the material model, an isotropic elasticity model was developed in order to capture the elastic behavior of 3D printed PA12 and a bilinear isotropic hardening model was employed to capture its plastic behavior until the ultimate stress (31.8 MPa) with a tangent modulus of 100MPa. Moreover, a mesh sensitivity analysis was performed focusing on equivalent von-Mises stresses in order to obtain mesh-independent results. The convergence analysis revealed that a computation mesh of tetrahedral elements with a minimum size of 1mm sufficiently provides reliable and mesh-independent results. Finally, for the boundary conditions of the FEM, the mounting holes were set fixed (zero degrees of freedom) and as a loading condition, a universal static pressure of 13 bar was set normalized on the internal fluid channels of the air manifold.

3. RESULTS AND DISCUSSION

After the comprehensive presentation of the applied methodology, techniques and materials, the next step is the demonstration of the study through a step-by-step process. Therefore, initially, the commercial design of the selected air-manifold was evaluated through the developed FEM applying the PA12 as construction in order to verify the sufficient structural integrity of the proposed material. Figure 4 shows the corresponding equivalent von-Mises contours at 13 bar internal pressure. For this analysis, it is revealed that manifolds constructed with PA12 can sufficiently withstand the applied loads. Moreover, it is obvious that a significant volume of the manifold reveals near to zero von-Mises stresses indicating that these regions can be removed without compromising the manifold's overall mechanical performance.

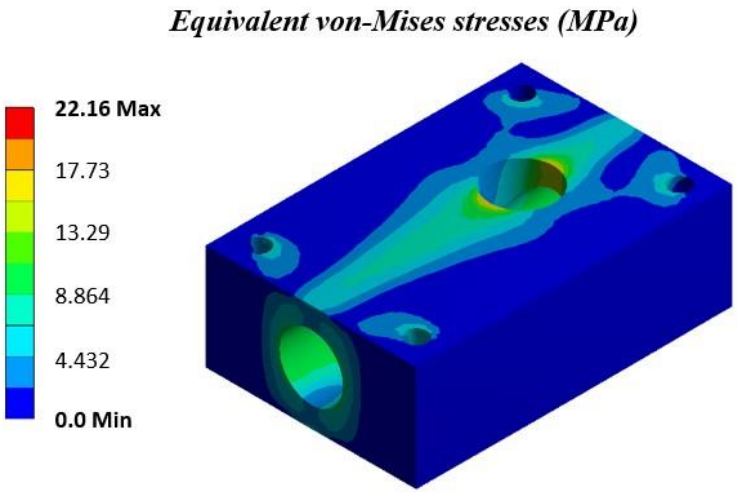

Fig. 4. Equivalent von-Mises stress contour for the initial design of the manifold constructed with PA12 and with loading condition at 13 bars

Towards this direction, a topology optimization process was performed utilizing a density-based approach and more specifically a Solid Isotropic Material with Penalization method (SIMP) algorithm via the nTopology platform. Figure 5a illustrates the optimized design of the manifold compared to the initial one. As it was expected the majority of regions that exhibited zero or low stresses were removed leading to a design with significantly lower volume and mass. Indicatively, the expected volume of this new design is 17.5 cm^3. Furthermore, in Figure 5b, the equivalent von-Mises stresses for the optimized design are presented. From this contour plot, it is derived that the new design concentrates stresses that exceed the yield strength of the construction at 28 MPa indicating that the component exhibits plastic deformations. However, the maximum observed stress is significantly lower than the UTS of the material showing that the optimized design can withstand the loads without causing total failure. These acquired results lead to the conclusion that the developed design of the manifold should be further optimized enhancing the structural integrity of regions with high stress concentration.

Driven by the stress results of the optimized design, it is necessary to improve the strength of the long region of the manifold and the regions of the front and bottom port tubes. To address this issue, the idea was to integrate structural ribs on the surface of the object. This became feasible by designing and implementing a conformable surface lattice structure on the area of interest. As it was aforementioned, the selected lattice structure was a triangular honeycomb and it was applied to all regions that showed increased stress concentration. Figure 6 shows

the 3D model of this advanced design coupled with the corresponding equivalent von-Mises stress contour. It is worth mentioning that the following design has a volume of 19.7 cm^3. For the FEA's results, it can be derived that the stresses were uniformly distributed within the volume of the manifold without observing any stress singularities or stress peaks due to the existence of the lattice grid. Moreover, the maximum stress was revealed at 21.82 MPa, i.e. lower than the yield strength of the material, indicating the flawless operation of the developed design under realistic conditions.

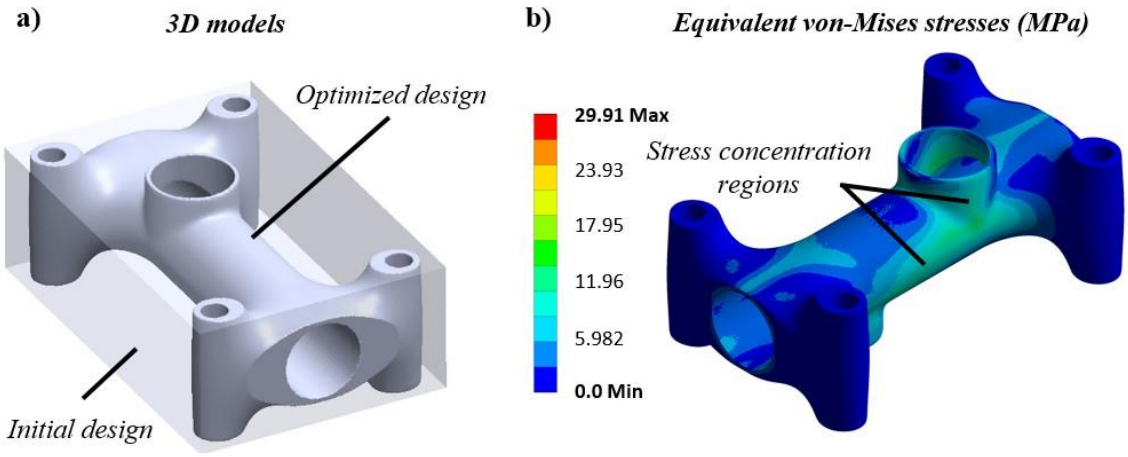

Fig. 5. a) 3D model of the optimized design compared to the initial one; b) Equivalent von-Mises stress contour for the optimized design of the manifold constructed with PA12 and with loading condition at 13 bars

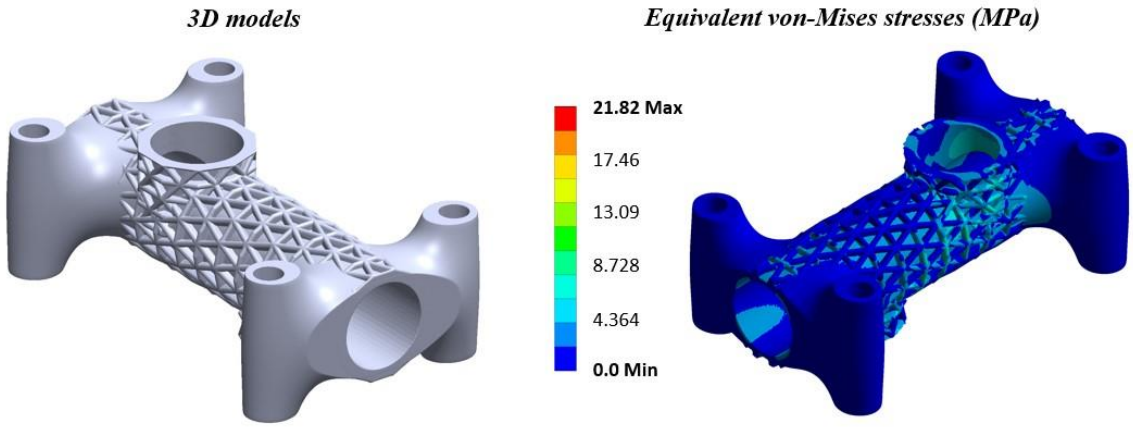

Fig. 6. 3D model of the optimized design integrated with surface lattice structure and the corresponding equivalent von-Mises stress contour

Proceeding one step beyond the computational analysis of the air manifold, the current study fabricated both versions of the optimized manifold's designs. Figure 7 shows indicative images of the 3D printed air manifolds. The 3D printing process for both design versions was around 20 hours. The produced 3D prints were fabricated without any issue and without observing any visible defects on their surfaces. In addition, Table 3 lists the corresponding volume, mass, percentage of mass reduction and factor of safety for all versions of the designed air manifold. From this information, it is obvious that the integration of conformable surface lattice structure on the optimized manifold's design enhanced the strength of the part by increasing the factor of safety by 37.1% at the same time the part's volume rose by only 12.5%. In addition, it is worth noting that the overall volume reduction from the initial to the final version of the manifold reached up to 75.5%. Finally, the cost of the 3D printed manifold was calculated at around 5€ (for only one part), with the cost of feedstock material constituting around 50% of the overall cost. With proper nesting and stacking process of the parts inside the building volume, it is estimated that this cost can be reduced by up to 30%.

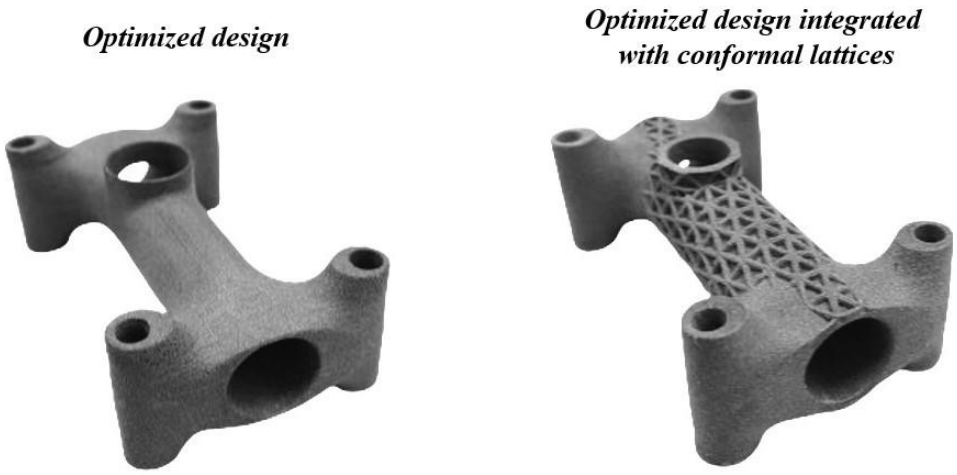

Fig. 7. 3D printed parts of the optimized version (left) and of the optimized version integrated with conformal lattices (right) for the examined manifold

Table 3. Volume, mass and factor of safety values for all examined versions of the air manifold

Designs	Volume	Mass	Difference	Factor of safety
Initial version	80.5 cm^3	78.09 gr	-	1.02
Optimized version	17.5 cm^3	16.98 gr	78.3 %	0.76
Final version	19.7 cm^3	19.11 gr	75.5%	1.04

4. CONCLUSIONS

In conclusion, the integration of topology optimization processes, DfAM and AM techniques marks a significant advancement in the design and production of mechanical components. This study showcases a comprehensive workflow for redesigning and optimizing a low-pressure air manifold, presenting the potential benefits of this approach. By leveraging iterative FEAs and employing novel surface-architected materials, the manifold's design achieved enhanced structural integrity and with a weight reduction of up to 75.5%. Furthermore, the utilization of the SLS 3D printing technique with PA12 as construction material supports the feasibility and cost-effectiveness of this methodology. It is important to note that the outlined workflow presents an indicative design roadmap applicable to a broad range of 3D-printed mechanical parts, including hydraulic manifolds, connectors, and nozzles. As design software continues to advance and manufacturing capabilities evolve, this integrated approach promises to drive further innovation in the optimization and production of lightweight, efficient, and economically viable mechanical components. Finally, it is worth noting that further research should be performed in this field with extensive experimental physical tests in order to ensure the structural integrity and the reliability of the 3D printed parts under real-life conditions.

Funding: This paper was supported by the *Horizon 2020 PestNu project, grant number 101037128*.
Conflicts of Interest: There is no conflict of interest.

REFERENCES

1. Gibson, I., Rosen, D.W., Stucker, B. (2010). *Additive Manufacturing Technologies*; Springer: New York, NY, USA. https://doi.org/10.1007/978-1-4939-2113-3.
2. Frazier W.E. (2014). *Metal additive manufacturing: a review*. J Mater Eng Perform, 23, 1917–1928. https://doi.org/10.1007/s11665-014-0958-z.
3. Kladovasilakis, N., Charalampous, P., Kostavelis, I., Tzetzis, D., Tzovaras, D. (2021). *Impact of metal additive manufacturing parameters on the powder bed fusion and direct energy deposition processes: A comprehensive review*. Prog. Addit. Manuf., 6, 349–365. https://doi.org/10.1007/s40964-021-00180-8.
4. Berman, B. (2012) *3-D printing: The new industrial revolution*, *Business Horizons*, 55(2), 155-162. https://doi.org/10.1016/j.bushor.2011.11.003.
5. Oropallo, W., Piegl, L.A. (2016). Ten challenges in 3D printing. Engineering with Computers, 32, 135–148. https://doi.org/10.1007/s00366-015-0407-0.
6. Wohlers, T., Campbell, I., Diegel, O., Kowen, J., (2019). *Wohlers Report: Additive Manufacturing State of the Industry*, Annual Worldwide Progress Report, ISBN 978-0-9913332-5-7.
7. Boothroyd, G. (1994) *Product design for manufacture and assembly*, Comput. Des., 26(7), 505–520. https://doi.org/10.1016/0010-4485(94)90082-5.

8. Yang, S., Zhao Y.F. (2015). *Additive manufacturing-enabled design theory and methodology: a critical review*, Int. J. Adv. Manuf. Technol., 80 (1), 327–342. https://doi.org/10.1007/s00170-015-6994-5.
9. Kumke, M., Watschke, H., Vietor, T. (2016). *A new methodological framework for design for additive manufacturing*, Virtual Phys. Prototyp., 11(1), 3. https://doi.org/10.1080/17452759.2016.1139377.
10. Thompson, M.K., Moroni, G., Vaneker, T., Fadel, G., Campbell, R.I., Gibson, I., Bernard, A., Schulz, J., Graf, P., Ahuja, B., Martina, F., (2016). *Design for additive manufacturing: trends, opportunities, considerations, and constraints*, CIRP Ann. Manuf. Technol., 65(2), 737–760. https://doi.org/10.1016/j.cirp.2016.05.004.
11. Ponche, R., Kerbrat, O., Mognol, P., Hascoet, J.Y. (2014) *A novel methodology of design for additive manufacturing applied to additive laser manufacturing process*, Robot. Comput. Manuf., 30(4), 389–398. https://doi.org/10.1016/j.rcim.2013.12.001.
12. Diegel, O., Schutte, J., Ferreira, A., Chan, Y.L. (2020). *Design for additive manufacturing process for a lightweight hydraulic manifold*, Additive Manufacturing, 36, 101446, https://doi.org/10.1016/j.addma.2020.101446.
13. Available from: https://jmcautomotiveequipment.com/rapid-air/rapid-air-90120-compressed-air-outlet-alum-block-only/, Accessed: 09/02/2024.
14 Kladovasilakis, N., Tsongas, K., Tzetzis, D. (2020). *Finite Element Analysis of Orthopedic Hip Implant with Functionally Graded Bioinspired Lattice Structures*. Biomimetics, 5, 44. https://doi.org/10.3390/biomimetics5030044.
15. Tcherniak, D. (2002). *Topology optimization of resonating structures using SIMP method*. Int. J. Numer. Methods Eng, 54, 1605–1622. https://doi.org/10.1002/nme.484.
16 Kladovasilakis, N., Tsongas, K., Karalekas, D., Tzetzis, D. (2022) *Architected Materials for Additive Manufacturing: A Comprehensive Review*, Materials, 15, 5919. https://doi.org/10.3390/ma15175919.
17. Pei, E., Kabir, I., Breški, T., Godec, D., Nordin, A. (2022) *A review of geometric dimensioning and tolerancing (GD&T) of additive manufacturing and powder bed fusion lattices*, Prog. Addit. Manuf., 7, 1297–1305. https://doi.org/10.1007/s40964-022-00304-8.
18. Kladovasilakis, N., Tsongas, K., Tzetzis D., (2023). *Development of novel additive manufactured hybrid architected materials and investigation of their mechanical behavior*, Mechanics of Materials, 176, 104525. https://doi.org/10.1016/j.mechmat.2022.104525.
19. Schneider, J., Kumar, S. (2020). *Multiscale characterization and constitutive parameters identification of polyamide (PA12) processed via selective laser sintering*, Polymer Testing, 86, 106357, https://doi.org/10.1016/j.polymertesting.2020.106357.

Received: February 23th, 2024 / Accepted: December 15th, 2024 / Paper available online: December 20th, 2024